18th Brazilian Congress of Thermal Sciences and Engineering
November 16-20, 2020 (online)

# ENC-2020-0201
# NUMERICAL ANALYSIS OF THE INFLUENCE OF CHAMBER SIZES AND TURBINE CHARACTERISTICS ON AN OSCILLATING WATER COLUMN WAVE ENERGY CONVERTER

**Guilherme Ferreira Wiener**
**Paulo Roberto de Freitas Teixeira**
Universidade Federal do Rio Grande, Engineering School, Av. Italia, km 8, Campus Carreiros, 96201-900, Rio Grande, RS, Brazil
gfw1994@gmail.com; pauloteixeira@furg.br

**Eric Lionel Didier**
Laboratório Nacional de Engenharia Civil, Hydraulics and Environment Department, Av. do Brasil, 101, 1700-066, Lisbon, Portugal
edidier@lnec.pt

***Abstract.*** *Nowadays, renewable energy is a topic widely discussed in scientific community. Specifically wave energy attracts attention because it has a high energy potential distributed throughout the planet. Oscillating Water Column (OWC) wave energy converter is one of the most studied devices that have promising perspectives to be installed commercially. This study aims investigating the influence of chamber sizes and turbine characteristics dimensions of an OWC device located at the southern Brazilian coast is carried out. Numerical simulations for incident waves with period T = 7 s and 10 s and height H = 1.5 m, by using the FLUENT® model, based on the finite volume method (VFM) are carried out. Efficiencies for different chamber sizes and Wells turbine characteristic relations (kt) in each incident wave are determined. The highest efficiencies were obtained by a chamber with 5 x 5 m and kt = 530 Pa.s/m³ in the case of an incident wave with T = 7s (52%), and 30 x 30 m and kt = 15 Pa.s/m³ at T = 10s (65%).*

***Keywords:*** *Wave energy Converter, Oscillating Water Column, Pneumatic Energy.*

## 1. INTRODUCTION

Alternatives to fossil fuels have been discussed since 1970 in Europe, due to the oil crisis, at a time when the nuclear energy received the most part of investments (Vicinanza et al., 2014). Disasters demotivated investments on it, so other sources of renewable energy gained prominence in the scientific community. Nowadays, the topic is so discussed that became one of the main goals of the 2030 Agenda, an official document from the United Nations, that aims at a more sustainable development of the planet, and that several world leaders have authenticated (UN, 2015). Another discussed point that shows the great need for other energy resources is that studies indicate that global demand tends to increase by up to 35% from 2010 to 2040 (Vicinanza et al., 2014).

Among many ways to obtain clean energy, the wave energy attracts attention due to its high energy potential, estimated at up to 3.7 TW of energy distributed across the planet, with South America holding approximately 531 GW, representing almost 14% of the global matrix (Mørk et al., 2010). However, in order to convert wave energy into electrical energy, it must be used some equipment with this purpose. Numerous models of these devices have been developed over the years, being called Wave Energy Converters (WEC) and can be divided into three categories, according to their operating principle: pressure difference, floating structures and impact (López et al., 2013).

The Oscillating Water Column (OWC) type device works by pressure difference and stands out for its simple functionality and theoretical understanding (Ning et al., 2016). It consists of a hollow structure with an opening below the submerged part of the OWC front wall. Incident waves make the water flows into the chamber. The water free surface inside the chamber is forced to oscillate, inducing an up-and-down air displacement that rotates the turbine (Liu et al., 2020). The concept of the OWC was created in the 1960's decade, by the Japanese scientist Yoshio Masuda, having your first prototype built in 1988, in the Islay's Island, with a nominal potential of 75 kW (Mustapa et al., 2017). Other physical models have been designed in different countries, as the device in Pico, Portugal, built in 1999 for reserch porpuses, with a nominal potential of 400 kW, where its objective was for research in the area, but ended in 2018 (WavEC, 2018).

Since construction of prototypes demand high costs, the use of numerical simulations, which are able to reproduce fluid structure interactions, is an alternative. Numerical simulation can be an interesting tool to perform an optimization of the OWC, since the great advantage of CFD (Computational Fluid Dynamics) is to be able to consider the structure at real scale (Dai et al., 2019).

Since OWC devices are robust reinforced concrete structures, their insertion in other marine structures, such as vertical breakwaters, is a good option, making the implementation of OWC more attractive (Mustapa et al., 2017). Dimensions of breakwaters allow that several wave energy converters are arranged in parallel along them. Shalby et al. (2019) reviewed the current concepts, proposals and research involving devices of the Oscillating Water Column type with several chambers, highlighting the advantages of greater power extracted by the set and better cost-benefit.

Following the hypothesis of implementing several OWC devices in parallel, one must question is: what are the dimensions of the OWC chamber that provide the best efficiency for converting wave energy, which could justify its economic viability? The aim of this work is to investigate the efficiency of OWC devices of different dimensions inserted in a hypothetical breakwater located on the south coast of Rio Grande do Sul state, Brazil. Lisboa et al. (2017) estimated the energy potential of the local waves and Lisboa et al. (2018) studied the energy extracted by an OWC device installed at this location, but with fixed dimensions of 10 x 10 m.

This study aims investigating efficiency of OWC devices for the two most energetic incident waves in the region ($T$ = 7 s, $H$ = 1.5 m and $T$ = 10 s and $H$ = 1.5 m) and three different turbine characteristic relations of a Wells turbine. Section 2 shows the study region in which the OWC device would be installed and the computational domain in which the numerical simulations are performed. The FLUENT® model, which is based on Reynolds Averaged Navier-Stokes equations and Volume of Fluid technique (RANS-VOF), is responsible by simulations of interactions between wave and structure. In this same section, FLUENT® boundary conditions and applied parameters are described. In section 3, results of tests are shown. In section 4, conclusions of the study are exposed.

## 2. METHODOLOGY

### 2.1 Case studies

Lisboa et al. (2017) studied the potential of wave energy near the city of São José do Norte, located in Rio Grande do Sul state (RS), Brazil. Characteristics of incident waves and wave power in the southern Brazilian coast by 10-year hindcast (1997 to 2006) were shown by the authors. Mike 21 SW was employed to model the wave propagation by using reanalysis wave data from Wavewatch III and wind data from the National Center for Environmental Predictions (NCEP). A matrix with the occurrence frequency of each wave period and height that composes the annual-averaged wave energy distribution of the region was determined. Figure 1a shows part of the southern coast of Brazil, highlighting the area of the highest energy potential, São José do Norte (SJN). Figure 1b shows the average distribution of wave energy at this local. In this study, two waves with the highest energy potential, that have periods of $T$ = 10 s and $T$ = 7 s, both with the wave height of $H$ = 1.5 m, are investigated.

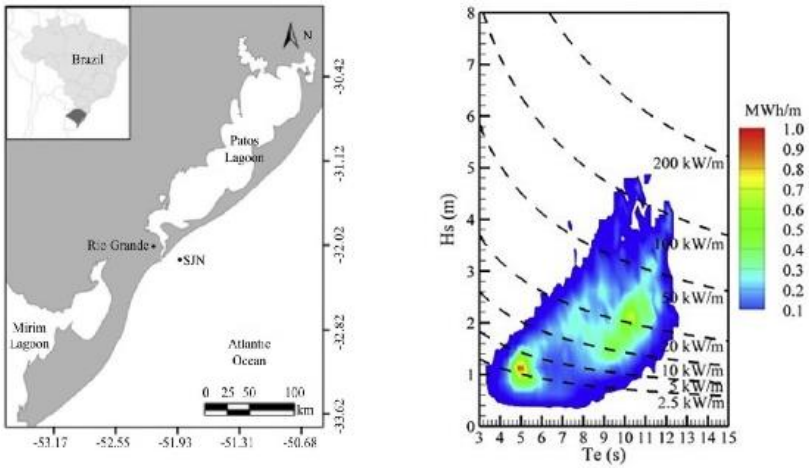


Figure 1. Study region (a) on a map and (b) annual-averaged distribution of sea wave energy in São José do Norte, Brazil. (Lisboa et al., 2017)

Lisboa et al. (2018) determined efficiency of an OWC Wave Energy Converter in this region by applying the FLUENT® model. The computational domain was composed by a flume with a OWC device at its end with fixed dimensions of 10 m length (*CL*), 10 m wide (10x10) and 16 m high (Fig. 2). The flume has a length of 4*L* and a depth of 14 m; it includes a slope of 30 m and an OWC device is inserted at its end (at 10 m depth). In this study, every computational domain geometry is the same used by Lisboa et al. (2018) (Fig. 2), except the chamber size, which are 5x5, 10x10, 15x15, 20x20, 25x25 and 30x30.

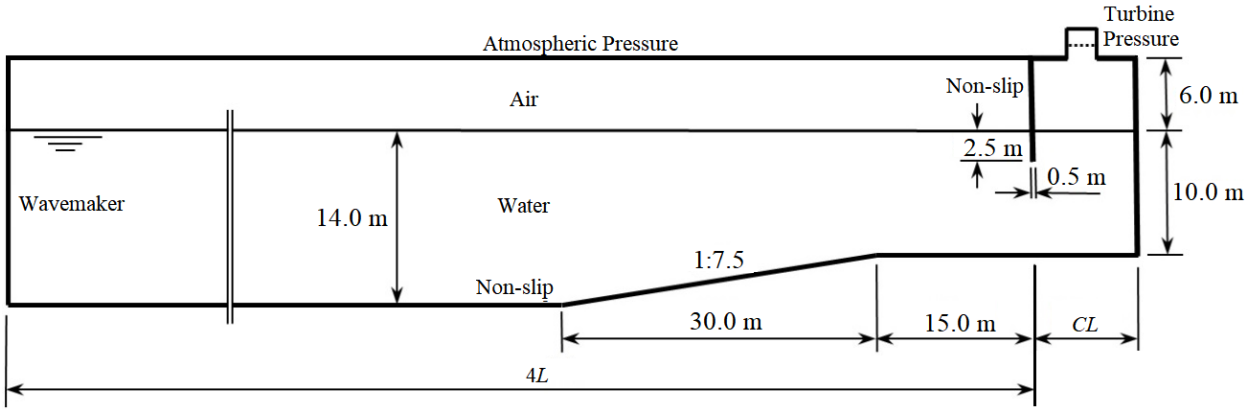


Figure 2. Computational domain and boundary conditions of the case study.

Efficiency of each OWC configuration is calculated considering the absorbed power in relation to the incident wave power over the device. The time-averaged wave power of monochromatic waves per unit width ($P_w$) is calculated by Eq. (1) (Dean and Dalrymple, 2000):

$$P_w = \left(\frac{\rho_w g^2}{32\pi} H^2 T\right)\left(1 + \frac{2kh}{sinh\, 2kh}\right) tanh\, kh \tag{1}$$

where $\rho_w$ is the specific mass of the water, $g$ is the gravitational acceleration, $H$ is the wave height and $T$ is the wave period. The incident wave power over the OWC device is determined considering its width.

In this study, the measurement of the efficiency is related to the pneumatic power. The time-averaged pneumatic power inside the chamber, $P_p$, is given by Eq. (2) (Torres, 2018):

$$\bar{P}_p = \frac{1}{T}\int_T Q_t(p - p_0)dt \tag{2}$$

where $Q_t$ is the turbine flow, $p$ is the air pressure inside the chamber and $p_0$ is the atmospheric pressure.

Therefore, efficiency of each case, that is the relation between the time-averaged pneumatic and incident wave powers, is given by:

$$\varepsilon = \frac{P_p}{P_w} \tag{3}$$

It is important emphasizing that, considering that it is possible to construct a cluster of OWC's in parallel along the breakwater, the absolute value of the time-averaged pneumatic power is not appropriate to this comparison. Therefore, the more adequate parameter to be used in this analysis is the efficiency determined by Eq. (3).

For the Wells turbine, the relationship between the pressure difference imposed by the turbine and the flow is linear, given by Eq. (4) (Torres et al., 2018):

$$kt = \frac{p - p_0}{Q_t} \tag{4}$$

where $kt$ is the turbine characteristic relation and $Q_t$ is the turbine flow. The characteristic relation of the turbine depends on its rotational speed and its diameter:

$$kt = \frac{\rho N}{KD} \tag{5}$$

where $N$ and $D$ are rotational speed and diameter of the turbine, respectively, $\rho$ is a specific mass of reference and $K$ is a constant characteristic of the turbine curve, which is 0.6803 in this case (Falcão and Justino, 1999). The rotational speed has an upper limit to avoid high level of vibrations. Torres et al. (2018) considered the maximum tangential velocity of the turbine rotor ($ND/2$) of 150 m/s and the minimum one of 50% of the maximum value. Therefore, considering practical values of turbine diameter ranged from 0.75 to 4.0 m, the range of $kt$ is from 15 to 960 Pa.s/m³, approximately. In this study, analyzes are carried out for $kt$ equals to 15, 530 and 960 Pa.s/m³, which are correspondent to turbine diameters around 0.75, 0.75–1.00 and 4.00 m, respectively.

## 2.2 Governing equations

The FLUENT® model is based on the continuity equation (mass conservation) and momentum equations (Navier-Stokes) that, for an incompressible and bidimensional flow, are (Versteeg e Malalasekera, 1995):

$$\frac{\partial u_i}{\partial x_i} = 0 \tag{6}$$

$$\frac{\partial \rho u_i}{\partial t} + u_j \frac{\partial \rho u_i}{\partial x_j} = -\frac{\partial p}{\partial x_i} + \rho g_i + \frac{\partial \tau_{ij}}{\partial x_j} \tag{7}$$

$$\tau_{ij} = \mu \left( \frac{\partial u_i}{\partial x_j} + \frac{\partial u_j}{\partial x_i} \right) \tag{8}$$

where $i, j = 1, 2$ for 2D flow, $\rho$ is the specific mass of the fluid, $g_i$ are the gravitational acceleration components, $u_i$ are the velocity components, $p$ is the pressure, $\mu$ is the dynamic viscosity and $\tau_{ij}$ is the viscous stress tensor. The finite volume method is used on the computational solver of those differential equations.

Reynolds Averaged Navier-Stokes equations (RANS) are used for turbulent flows, which instantaneous pressure and velocity fields are separated into average and fluctuating, and time-averaged Navier-Stokes equations are used. This process introduces Reynolds stress terms associated with turbulence. In this study, the standard model $k$-$\varepsilon$ is used to relate the Reynolds stresses and flow variables and, consequently, to close the system equations.

The Volume of Fluid method (VoF) is used to treat the free surface (Hirt and Nichols, 1981). On this method, the volume fraction, represented by α, has the value of 0 to the air phase and 1 to the water phase, and any value between 0 and 1 represents a proportion of the two phases on that cell. The value that locates the position of the free surface is α = 0.5. The variable α is calculated at each instant by the transport equation:

$$\frac{\partial \alpha}{\partial t} + u_j \frac{\partial \alpha}{\partial x_j} + 0 \tag{9}$$

## 2.3 Numerical conditions

At the wave maker, velocity components and elevation of the free surface, based on linear wave equations, are imposed, according to Dean e Dalrymple (2000), by means of User-Defined Functions (UDF) (Fig. 2). An active absorption method is employed in order to avoid reflected waves into the flume (Teixeira et al, 2013, Torres et al., 2016, Mendonça et al., 2018 and Gaspar et al., 2020). The non-slip condition is imposed on the walls of the chamber and on the bottom of the flume. In the upper boundary, the atmospheric pressure is imposed as pressure condition (101325 Pa). At the top of the OWC, the turbine pressure is imposed at each instant, calculated by Eq. (4), by means of UDF. Although the mathematical model is 2D, the flow rate measured at each instant to be used in Eq. (4) consider the width of the chamber *CW*.

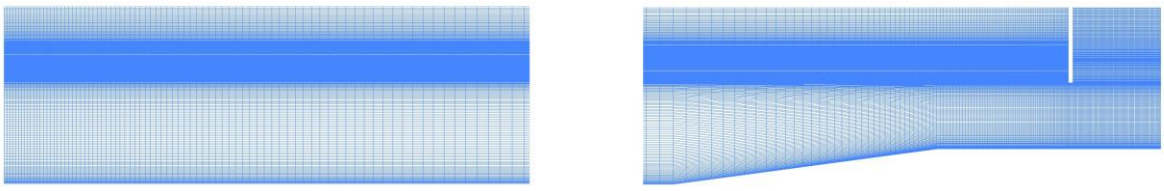

(a) (b)

Figure 3. Mesh in (a) wavemaker zone and (b) OWC zone for an incident wave of $T$ = 10 s and $H$ = 1.5 m and a chamber with $CL$ = 10 m

Figure 3 shows the mesh (quadrilateral cells) employed for an incident wave of $T$ = 10 s and $H$ = 1.5 m and a chamber length with $CL$ = 10 m. The horizontal discretization is divided into 70 cells per wavelength. Along the flume, in a zone around the free surface with height of 2 $H$, there are 50 cells in the vertical direction. Inside the chamber, both height and length of the cell are equivalent to 0.125m. Meshes have an average of 100 thousand cells (there is one different mesh for each chamber size). The time step is equal to $T$/640 and the total flow duration is 36 $T$, which is sufficient to stabilize the flow. The SIMPLEC algorithm (Semi-Implicit Method for Pressure Linked Equations-Consistent) is used for the pressure-velocity coupling and a second order implicit scheme is applied to time integration and turbulence model $\kappa$-$\varepsilon$. The volume fraction of each cell is calculated by the Modified HRIC (High Resolution Interface Capturing) to determine the free surface of the flow. The PRESTO! (PREssure STaggering Option) method is used for spatial discretization of pressure and the under-relaxation factor of momentum, volume fraction, pressure and $\kappa$-$\varepsilon$ are the value of 1. Teixeira et

al. (2013), Dias et al. (2015), Gonçalves et al. (2020) and Gaspar et al. (2020) validated and applied both boundary conditions and parameters used in this Section.

## 3. RESULTS AND DISCUSSION

Figure 4 shows velocity magnitude contours and streamlines at 5 different instants during a wave period, for a wave of $T$ = 10s and $H$ = 1.5m, with a $kt$ = 530 Pa.s/m³ and a chamber with $CL$ = 5 m. The first instant marks the zero up-crossing of the free surface inside the chamber. It can be observed that the highest velocity magnitude occurs under the front wall of the chamber. A vortex is formed inside the chamber during the changing of inflow to outflow ($t = T/4$). On the bottom corner of the device, the velocity magnitude is low.

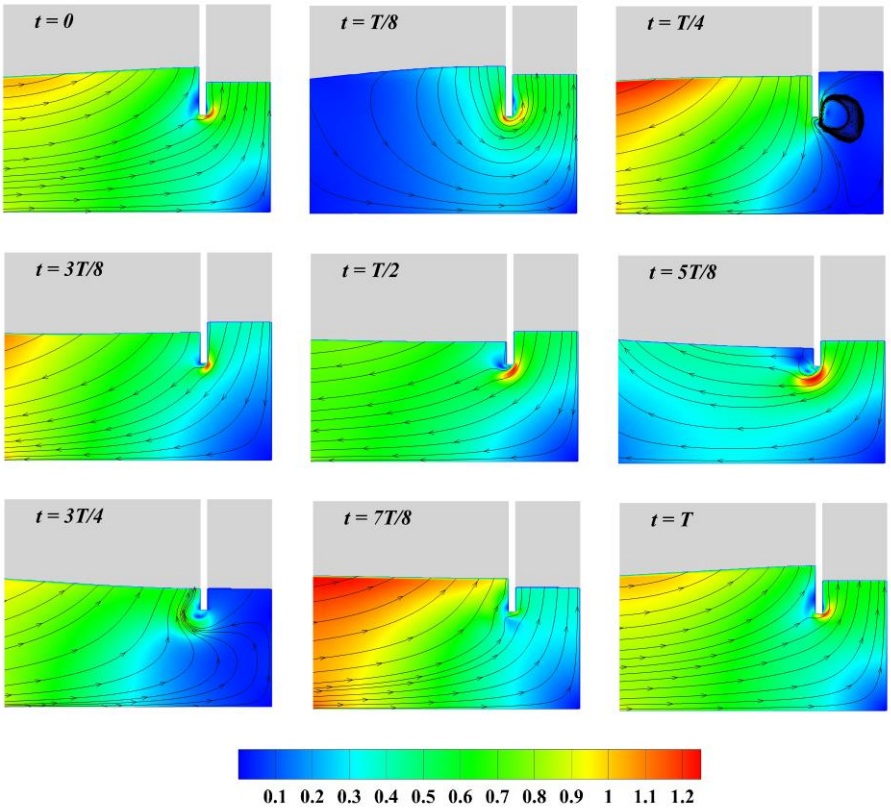


Figure 4. Velocity magnitude contours and streamlines at five instants during a wave period due to an incident wave of $T$ = 10 s and $H$ = 1.5 m, $kt$ = 530 Pa.s/m³ and a chamber with $CL$ = 5 m

Figure 5 shows velocity magnitude contours and streamlines in a chamber with $CL$ = 30 m. It can be notice that the highest velocity magnitude occurs under the front wall of the chamber as occurred in the previous case. On the bottom corner of the device, the velocity magnitude is also low. It is clear that, in this chamber, velocity magnitude inside the device is smaller than that of previous case.

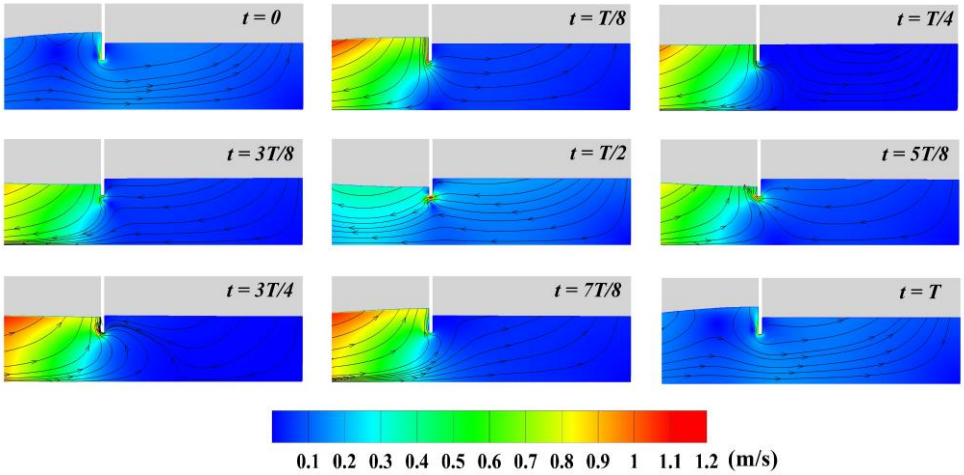


Figure 5. Velocity magnitude contours and streamlines at five instants during a wave period due to an incident wave of $T$ = 10s and $H$ = 1.5m, $kt$ = 530 Pa.s/m³ and a chamber with $CL$ = 30 m

Figures 6 shows time series of free surface elevation and air pressure inside the chamber and pneumatic power for chambers 5x5 and 30x30, respectively. In this case, the relation between the wave height inside the chamber and the height of the incident wave are 1.23 and 0.05 for chambers 5x5 and 30x30, respectively. Air pressure inside the chamber for chamber 5x5 has maximum and minimum amplitudes of 8.1 and -7.3 kPa, respectively. In the case of chamber 10x10, these values are 12.0 and -11.8 kPa. In both cases, the maximum amplitude of the air pressure (inhalation) is higher than the minimum one (exhalation); in consequence, maximum amplitude of pneumatic power is higher than minimum one (124.6 and 99.0 kW in the case of 5x5 and 268.7 and 248.2 kW in 30x30).

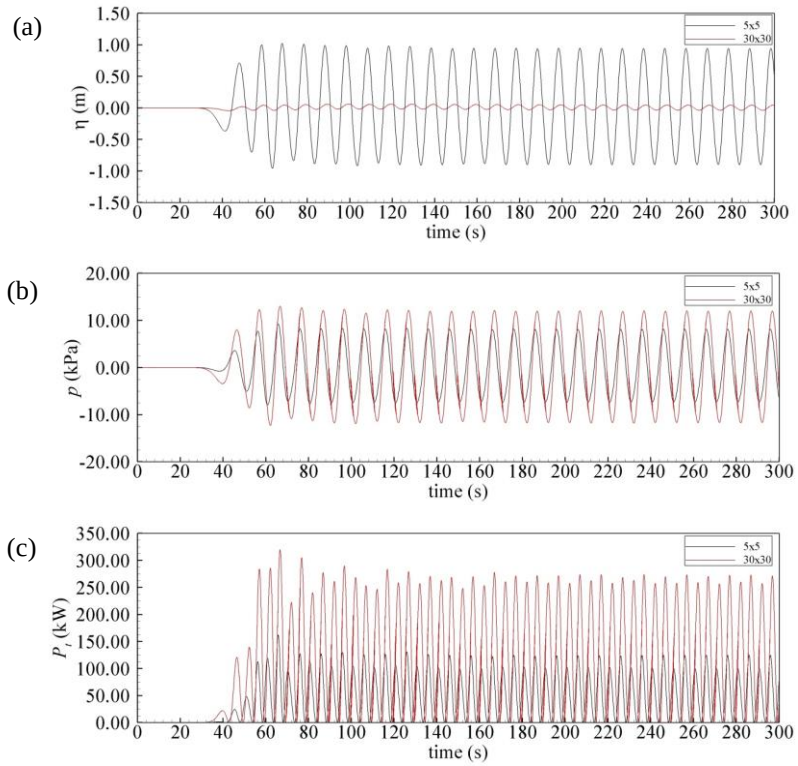


Figure 6. Time series of free surface elevation (a) and air pressure (b) inside the chamber and (b) pneumatic power for an incident wave of T = 10 s, H = 1.5 m, a turbine with kt = 530 Pa s-3 and chambers (a) 5x5 and (b) 30x30

Table 1 shows time-averaged wave power (Eq. (1)) and efficiency (Eq. 3)) considering chambers with 5, 10, 15, 20, 25 and 30 m section sizes and turbine characteristic relations of 15, 530 and 960 Pa.s/m³ for incident waves of $T$ = 7 s and $T$ = 10 s, where both heights are $H$ = 1.5 m. Figure 7 shows curves of $kt$ versus ε for both incident waves based on values of Tab. 1. In the case of incident wave with $T$ = 7 s, chamber 5x5 reached the highest efficiency at $kt$ = 530 Pa.s/m³, which

is 52%. Chamber 30x30 had efficiency almost null for every values of *kt*. The reason is that the chamber length is almost a half of the wave length, which is 66.40 m, calculated based on the liner theory (Dean and Dalrymple, 2000). It can be observed that, in this range of *kt*, the relation between the maximum efficiency and the chamber size is not linear, i.e., in progressive order of maximum efficiency, the chamber sizes (except 30x30) are: 25x25 (25%), 10x10 (37%), 15x15 (43%), 20x20 (45%), and 5x5 (52%).

In the case of incident wave with $T$ = 10 s, the highest efficiency was 65% by chamber 30x30 with $kt$ = 15 Pa.s/m³, that is higher than that obtained in wave with $T$ = 7 s. However, chamber 25x25 reached efficiency around 64%, which is similar. The lowest one occurred for chamber 5x5, around 4% at $kt$ = 15 Pa.s/m³. In this case, the progressive sequence of the higher maximum efficiency was: 5x5 (4%), 15x15 (39%), 10x10 (43%), 20x20 (54%), 25x25 (64%), and 30x30 (65%). It can be notice that chamber size of 15x15 has lowest maximum efficiency than that of chamber size 10x10.

Considering both cases, it can be observed that incident waves with higher periods (higher wave lengths) tend to provide higher efficiencies in larger chamber sizes and lower values of *kt*. According to Eq. (5), it is possible to conclude that low values of *kt* implies in high values of the turbine diameter, that is expected, since the higher chamber sizes have higher air flow rate inside the chamber.

Results obtained in this analysis show that there are different optimal chamber sizes and turbine characteristic relation for each incident wave characteristic. Moreover, the chamber size that reached the highest efficiency in one wave has low efficiency in the other one. In these cases, chamber 5x5 has the highest efficiency at $T$ = 7 s, but efficiency is only 5% at $T$ = 10 s. Besides, chamber 30x30 that has the highest efficiency at $T$ = 10 s (65%), shows efficiency practically null at $T$ = 7 s. Therefore, the best solution is one that has the maximum efficiency calculated considering the weight of the occurrence frequency of each incident wave of the average annual sea state of the region.

The importance of this study is noticed if results are compared with those obtained by Lisboa et al. (2018), in which a fixed chamber size of 10x10 m was used. It was shown that the chamber size of 10x10 does not provide the highest efficiency in both incident waves. Therefore, the optimal configuration must be determined including the chamber size of the OWC device.

Table 1. Time-averaged wave power $P_w$ and efficiency $\varepsilon$ for each wave period $T$, chamber length and width $CL$ x $CW$ and Wells turbine characteristic relation $kt$.

| $T$ (s) | $CL$ x $CW$ (m x m) | $P_w$ (kW) | $\varepsilon$ (%) | | |
|---|---|---|---|---|---|
| | | | $kt$ = 15 Pa.s/m³ | $kt$ = 530 Pa.s/m³ | $kt$ = 960 Pa.s/m³ |
| 7 | 5 x 5 | 89.88 | 7.80 | 52.22 | 39.50 |
| 7 | 10 x 10 | 179.77 | 27.11 | 38.20 | 23.92 |
| 7 | 15 x 15 | 269.65 | 42.45 | 27.81 | 16.69 |
| 7 | 20 x 20 | 359.53 | 45.36 | 21.61 | 12.72 |
| 7 | 25 x 25 | 449.42 | 27.58 | 17.37 | 10.15 |
| 7 | 30 x 30 | 539.90 | 0.08 | 1.00 | 1.35 |
| 10 | 5 x 5 | 121.00 | 3.60 | 45.99 | 40.93 |
| 10 | 10 x 10 | 242.00 | 19.37 | 44.17 | 28.63 |
| 10 | 15 x 15 | 363.00 | 39.13 | 33.50 | 20.40 |
| 10 | 20 x 20 | 484.01 | 53.87 | 26.56 | 15.79 |
| 10 | 25 x 25 | 605.01 | 63.87 | 21.92 | 12.85 |
| 10 | 30 x 30 | 726.01 | 64.79 | 18.64 | 10.85 |

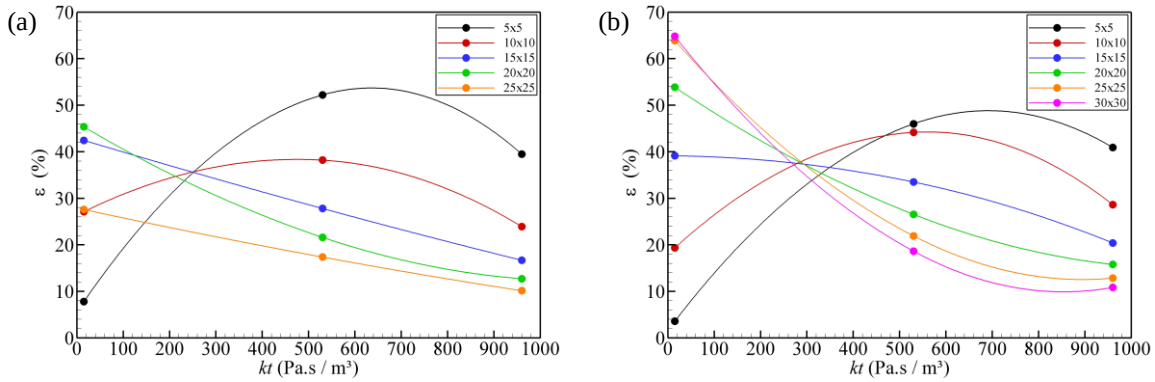


Figure 7. Efficiency versus $kt$ for different chamber dimensions in a wave of $T$ = 7s and $H$ = 1.5m

## 4. CONCLUSIONS

In this study, a numerical analysis of the influence of chamber sizes and turbine characteristics of an OWC wave energy converter device, located at southern Brazilian coast, on efficiency was carried out. Two most energetics incident waves were simulated ($T$ = 7 and 10 s, both with $H$ = 1.5 m).

Maximum efficiencies of 52% ($T$ = 7 s) and 65% ($T$ = 10 s) were found for chamber sizes and Wells turbine characteristic relation of 5x5 and $kt$ = 530 Pa.s/m³, and 30x30 and $kt$ = 15 Pa.s/m³, in incident waves with $T$ = 7 and 10 s, respectively. It was noticed that incident waves with higher periods (higher wave lengths) tended to provide higher efficiencies in larger chamber sizes and lower values of $kt$ (higher turbine diameters). Besides, the chamber size that reached the highest efficiency due to the incidence of one wave had low efficiency in the other.

This study shows the importance of considering simultaneously chamber sizes and turbine characteristics to evaluate the optimal configuration of a cluster of OWC devices inserted in a breakwater. Moreover, the best solution is one that has the maximum efficiency calculated considering the weight of the occurrence frequency of each incident wave of the averaged-annual sea state of the region.

## 5. REFERENCES

DAI, S. et al. Investigation on the hydrodynamic scaling effect of an OWC type wave energy device using experiment and CFD simulation. **Renewable Energy**, v. 142, p. 184–194, 2019.

DEAN, R.G.; DALRYMPLE, R.A. **Water wave mechanics for engineers and scientists**, London: World scientific publishing Co. Pte. Ltd, 2000.

FLUENT, 2016. User's Guide, ANSYS Inc.

FALCÃO, A. F. D. O.; JUSTINO, P. A. P. OWC wave energy devices with air flow control. **Ocean Engineering**, v. 26, p. 1275–1295, 1999.

GASPAR, L. A.; TEIXEIRA, P. R. F.; DIDIER, E. Numerical analysis of the performance of two onshore oscillating water column wave energy converters at different chamber wall slopes. **Ocean Engineering**, v. 201, n. June 2019, p. 107119, 2020.

GONÇALVES, R. A. A. C.; TEIXEIRA, P. R. F.; DIDIER, E. Numerical analysis of the influence of air compressibility effects on an oscillating water column wave energy converter chamber. **Renewable Energy**, v. 153, p. 1183–1193, 2020.

HIRT, C. W.; NICHOLS, B. D. Volume of Fluid (VOF) Method for the Dynamics of Free Boundaries. **Journal of computational physics**, v. 39, p. 201–255, 1981.

J. DIAS, A. MENDONÇA, E. DIDIER, M.G. NEVES, J. M. P. C. Application of Urans-Vof Models in Hydrodynamic Study of Oscillating Water Column. v. 467, n. October, p. 2–3, 2015.

LISBOA, R. C. et al. Numerical evaluation of the power output of an oscillating water column wave energy converter installed in the southern Brazilian coast. **Energy**, v. 162, p. 1115–1124, 2018.

LISBOA, R. C.; TEIXEIRA, P. R. F.; FORTES, C. J. Numerical evaluation of wave energy potential in the south of Brazil. **Energy**, v. 121, p. 176–184, 2017.

LIU, Z. et al. Overall performance evaluation of a model-scale OWC wave energy converter. **Renewable Energy**, v. 149, p. 1325–1338, 2020.

LÓPEZ, I. et al. Review of wave energy technologies and the necessary power-equipment. **Renewable and Sustainable Energy Reviews**, v. 27, p. 413–434, 2013.

MENDONÇA, A. et al. An integrated tool for modelling oscillating water column (OWC) wave energy converters (WEC) in vertical breakwaters. **Journal of Hydro-Environment Research**, v. 19, p. 198–213, 1 mar. 2018.

MØRK, G. et al. Assessing the global wave energy potential. **Proceedings of the International Conference on Offshore Mechanics and Arctic Engineering - OMAE**, v. 3, n. 2008, p. 447–454, 2010.

MUSTAPA, M. A. et al. Wave energy device and breakwater integration: A review. **Renewable and Sustainable Energy Reviews**, v. 77, n. September, p. 43–58, 2017.

NING, D. Z.; WAANG, R.Q.; GOU, Y.; ZHAO, M.; BIN, T. Numerical and experimental investigation of wave dynamics on a land-fixed OWC device. **Energy**, v. 115, p. 326-337, 2016.

ONU. **Transformando nosso mundo: a agenda 2030 para o desenvolvimento sustentável**. Available in: <http://www.un.org/ga/search/view_doc.asp?symbol=A/RES/70/1&Lang=E>.

SHALBY, M.; DORRELL, D. G.; WALKER, P. Multi–chamber oscillating water column wave energy converters and air turbines: A review. **International Journal of Energy Research**, v. 43, n. 2, p. 681–696, 2019.

TEIXEIRA, P. R. F. et al. Numerical simulation of an oscillating water column device using acode based on Navier-Stokes equations. **Energy**, v. 61, p. 513–530, 2013.

TORRES, F. R.; TEIXEIRA, P. R. F.; DIDIER, E. Study of the turbine power output of an oscillating water column device by using a hydrodynamic – Aerodynamic coupled model. **Ocean Engineering**, v. 125, p. 147–154, 2016.

VERSTEEG, H. K.; MALALASEKERA, W. **An Introduction To Computational Fluid**. [s.l.] Longman Scientific & Technical, 1995.

VICINANZA, D. et al. Innovative rubble mound breakwaters for overtopping wave energy conversion. **Coastal**

**Engineering**, v. 88, p. 154–170, 2014.
WAVEC. **OWC Pico Power Plant**. Available in: <http://www.pico-owc.net/cms.php?page=616&wnsid=c84b02e823264521f7423e9ca9cf5b46>.

## 6. RESPONSIBILITY NOTICE

The authors are the only responsible for the printed material included in this paper.